AGU PUBLICATIONS

JGR

Journal of Geophysical Research: Oceans

RESEARCH ARTICLE

10.1002/2014JC009915

Key Points:
- Detailed pathways of basal meltwater from Antarctic ice shelves
- Pathways of basal meltwaters depend on formation site
- The basal meltwater has impacts on the Southern Ocean System

Correspondence to:
K. Kusahara,
kazuya.kusahara@lowtem.hokudai.ac.jp

Citation:
Kusahara, K., and H. Hasumi (2014), Pathways of basal meltwater from Antarctic ice shelves: A model study, *J. Geophys. Res. Oceans*, *119*, 5690–5704, doi:10.1002/2014JC009915.

Received 16 FEB 2014
Accepted 7 AUG 2014
Accepted article online 12 AUG 2014
Published online 3 SEP 2014
Corrected 10 OCT 2014

This article was corrected on 10 OCT 2014. See the end of the full text for details.

Pathways of basal meltwater from Antarctic ice shelves: A model study

Kazuya Kusahara[1] and Hiroyasu Hasumi[2]

[1]Institute of Low Temperature Science, Hokkaido University, Sapporo, Japan, [2]Atmosphere and Ocean Research Institute, The University of Tokyo, Chiba, Japan

Abstract We investigate spreading pathways of basal meltwater released from all Antarctic ice shelves using a circumpolar coupled ice shelf-sea ice-ocean model that reproduces major features of the Southern Ocean circulation, including the Antarctic Circumpolar Current (ACC). Several independent virtual tracers are used to identify detailed pathways of basal meltwaters. The spreading pathways of the meltwater tracers depend on formation sites, because the meltwaters are transported by local ambient ocean circulation. Meltwaters from ice shelves in the Weddell and Amundsen-Bellingshausen Seas in surface/subsurface layers are effectively advected to lower latitudes with the ACC. Although a large portion of the basal meltwaters is present in surface and subsurface layers, a part of the basal meltwaters penetrates into the bottom layer through active dense water formation along the Antarctic coastal margins. The signals at the seafloor extend along the topography, showing a horizontal distribution similar to the observed spreading of Antarctic Bottom Water. Meltwaters originating from ice shelves in the Weddell and Ross Seas and in the Indian sector significantly contribute to the bottom signals. A series of numerical experiments in which thermodynamic interaction between the ice shelf and ocean is neglected regionally demonstrates that the basal meltwater of each ice shelf impacts sea ice and/or ocean thermohaline circulation in the Southern Ocean.

1. Introduction

The Antarctic Ice Sheet is one of the most important subsystems in the Earth's climate, because the ice sheet mass balance has significant impacts on global mean sea level and on both global and local ocean circulations. In the reverse direction, changes in the Southern Ocean have been considered to play an important role in regulating the mass balance through processes at Antarctic ice shelves [*Dupont and Alley*, 2005; *Schoof*, 2007; *Rignot et al*., 2008; *Pritchard et al*., 2009, 2012].

The Antarctic Ice Sheet discharges approximately 2000–2500 Gt/yr of ice into the Southern Ocean under present-day conditions [*Rignot et al*., 2008, 2011]. The major ablation processes of the Antarctic Ice Sheet are due to the melting at ice shelf bases and calving of icebergs at ice shelf fronts. Melting at the ice shelf base is due to contact with relatively warm waters, which have a higher temperature than the in situ freezing point. Traditionally, the melting at ice shelf bases is believed to account for 20–40% of the total ice ablation, while calving icebergs account for the rest [*Jacobs et al*., 1992, 1996; *Hooke*, 2005]. However, recent studies of *Rignot et al*. [2013] and *Depoorter et al*. [2013] reported, from their accurate and high-resolution glaciological estimate, that basal melting accounts for more than half of Antarctic ice shelf mass loss. This indicates either that basal melting is more important than previously thought or that the melting at the Antarctic ice shelf bases has increased in recent decades. From the perspective of ocean boundary conditions, basal melting and calving contribute to the input of freshwater into the Southern Ocean.

Recent observations in contrast to historical data clearly show that the Southern Ocean is freshening in the surface/subsurface and bottom layers [*Jacobs et al*., 2002; *Jacobs*, 2004; *Boyer et al*., 2005; *Aoki et al*., 2005; *Rintoul*, 2007; *Helm et al*., 2010; *Jacobs and Giulivi*, 2010; *Hellmer et al*., 2011; *Shimada et al*., 2012; *Huhn et al*., 2013]. Satellite analyses show a significant increase in ice discharge into the Southern Ocean [*Rignot et al*., 2008, 2011] and a pronounced thinning over and near fringing ice shelves [*Pritchard et al*., 2009, 2012], indicating a more active interaction between the ice shelf base and ocean. Observational evidence of the Antarctic Ice Sheet and Southern Ocean suggests that the enhanced melting of continental ice contributes to

the Southern Ocean freshening [*Hellmer and Jacobs*, 1994; *Shepherd et al*., 2004; *Helm et al*., 2010; *Jacobs and Giulivi*, 2010].

Iceberg locations have been observed by satellite, and the associated meltwater distribution is estimated from both observation and modeling techniques [*Tournadre et al*., 2008, 2012; *Gladstone et al*., 2001; *Silva et al*., 2006; *Jongma et al*., 2009; *Martin and Adcroft*, 2010]. In contrast, meltwater distribution released from the Antarctic ice shelf bases is not well clarified by now.

Chemical tracers, such as oxygen, helium, and neon, are often used to trace the basal meltwater of Antarctic ice shelves in ocean water [*Schlosser*, 1986; *Schlosser et al*., 1990; *Jenkins and Jacobs*, 2008]. These observational techniques are applied to coastal waters near the sources around Antarctica. The signals of the meltwater are hardly detectable in offshore regions because mixing with ambient water dilutes the meltwater. *Rodehacke et al*. [2007] incorporated helium and neon into their model to investigate in detail the distribution of these tracers in basal meltwaters of Antarctic ice shelves. Their work was a pioneering modeling study of the basal meltwater. However, the horizontal resolution of their model is coarse (1.5–6.75° in longitude, $1.5^\circ \cos\phi$ in latitude); therefore, the model resolved only large ice shelves and did not well represent seafloor topography over the entire Southern Ocean. In reality, there are many small ice shelves around Antarctica, and regional ocean flows are controlled by finer bottom topography from a few to several tens of kilometers. Recent studies showed that the total amount of basal melting at small ice shelves is comparable to or even larger than that of the largest ice shelves [*Timmermann et al*., 2012; *Kusahara and Hasumi*, 2013; *Rignot et al*., 2013; *Depoorter et al*., 2013].

This study assesses the distribution of basal meltwaters of all Antarctic ice shelves by using a circumpolar coupled ice shelf-sea ice-ocean model. Basal meltwater is transported by ambient ocean circulations in the open ocean. The eastward flowing Antarctic Circumpolar Current (ACC) is the most prominent feature in the Southern Ocean and therefore plays an important role in distributing ocean tracers. Thus, we first investigate the ACC representation in the numerical model, comparing the boundaries and fronts inferred from hydrographic observations. Next, we cluster ice shelves into five groups and release an independent virtual tracer from each group to trace its basal meltwater and examine its behavior. The grouping is region based, and we can investigate detailed pathways of basal meltwater for each ice shelf group. Finally, we examine the impact of regional basal meltwater on sea ice and deep ocean thermohaline circulation fields.

2. Numerical Model and Experiments

2.1. A Coupled Ice Shelf-Sea Ice-Ocean Model

This study uses the circumpolar coupled ice shelf-sea ice-ocean model used in *Kusahara and Hasumi* [2013]. Only a brief outline of the model setup is presented here. The model domain is taken to be the Southern Ocean and an artificial northern boundary as a solid wall is placed at approximately 35°S. In the northernmost six grid cells, temperature and salinity are restored to the monthly mean climatology of the World Ocean Atlas 1998 [*Conkright et al*., 1998] throughout the water column with a damping time scale of 10 days.

The horizontal grid spacing over Antarctic coastal regions is between 10 and 20 km; thus, we represent almost all of the Antarctic ice shelves in a single model (Figure 1). The bathymetry and ice shelf draft are derived from the RTopo-1 data set [*Timmermann et al*., 2010]. This relatively high horizontal resolution enables us to simulate high sea ice production and dense water formation along the Antarctic coastal margins [*Marsland et al*., 2004; *Kusahara et al*., 2010, 2011]. However, it should be noted that this model does not resolve ocean eddies since the baroclinic Rossby radius of deformation ranges from a few kilometers in Antarctic coastal regions to 10–20 km in ACC regions [*Chelton et al*., 1998].

The ocean model includes the uniformly third-order polynomial interpolation algorithm for tracer advection [*Leonard et al*., 1993], isopycnal diffusion with the coefficient of 1.0×10^{1} m^2s^{-1}, isopycnal layer thickness diffusion with the coefficient of 1.0 m^2s^{-1} [*Gent et al*., 1995], and a surface mixed layer parameterization based on turbulence closure [*Noh and Kim*, 1999]. Under ice shelves, the surface mixed layer parameterization is neglected. For further details on the model setup, see *Kusahara and Hasumi* [2013].

We perform a 25 year simulation driven by present-day climate conditions. Surface boundary conditions are calculated from the atmospheric surface data set of *Röske* [2006]. After about 15 year

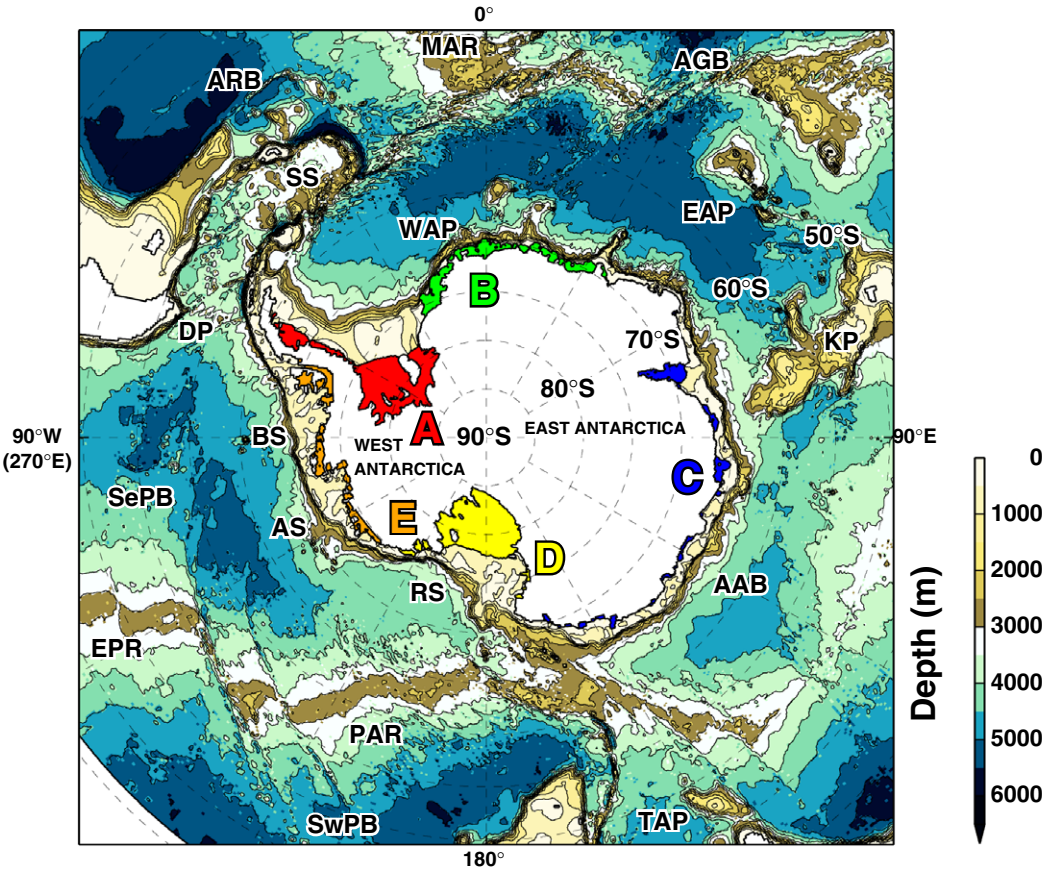

Figure 1. Bottom topography in the model. Ice shelf grouping (A–E) is indicated by color: the western and southern Weddell Sea (red, labeled by A), the eastern Weddell Sea (green, B), the Indian Sector (blue, C), the Ross Sea (yellow, D), and the Amundsen-Bellingshausen Seas (orange, E). ARB indicates the Argentine Basin, WAP the Weddell Abyssal Plain, MAR the Mid-Atlantic Ridge, AGB the Agulhas Basin, EAP the Enderby Abyssal Plain, KP the Kerguelen Plateau, AAB the Australian-Antarctic Basin, TAP the Tasman Abyssal Plain, RS the Ross Sea, PAR the Pacific-Antarctic Ridge, SwPB the Southwest Pacific Basin, AS the Amundsen Sea, BS the Bellingshausen Sea, EPR the East Pacific Rise, SePB the Southeast Pacific Basin, DP the Drake Passage, and SS the Scotia Sea.

integration, modeled ice shelf basal melting reaches a quasi steady state. The net amount of basal melting averaged over the last 10 years (16th–25th year) is 800 Gt/yr. The total basal melting in this model is consistent with previous observation-based and modeling estimates [*Kusahara and Hasumi*, 2013], and therefore, we consider that this model can roughly reproduce the basal melting of Antarctic ice shelves. However, it should be noted that the basal melting amount of the Antarctic ice shelves estimated from recent satellite data [*Rignot et al.*, 2013; *Depoorter et al.*, 2013] is larger than that in this model and previous literature.

2.2. Virtual Tracer for Basal Meltwater Released From Antarctic Ice Shelves

The basal meltwater flux at ice shelf bases is calculated by a three-equation scheme, based on a pressure-depending freezing point equation and conservation equations of heat and salinity [*Holland and Jenkins*, 1999]. We perform virtual tracer experiments, in which a tracer is released at the same rate as basal melting at ice shelf bases and is passively transported by modeled ocean flows, to investigate in detail the behavior of basal meltwaters.

For simplicity, we do not take account of exchanges of the virtual tracer between the ocean and sea ice/atmosphere. This treatment is the same as that for chemically inert tracers released from ice shelf bases [*Hellmer and Olbers*, 1989]. We perform a 10 year integration (16th-25th year) for virtual tracer experiments, starting from the end of the fifteenth year in the standard experiment. The initial condition for the virtual tracer is zero over the entire model domain. We categorize ice shelves into five groups based upon location (labels A–E in Figure 1) and independently release a virtual tracer for each group to investigate the behavior

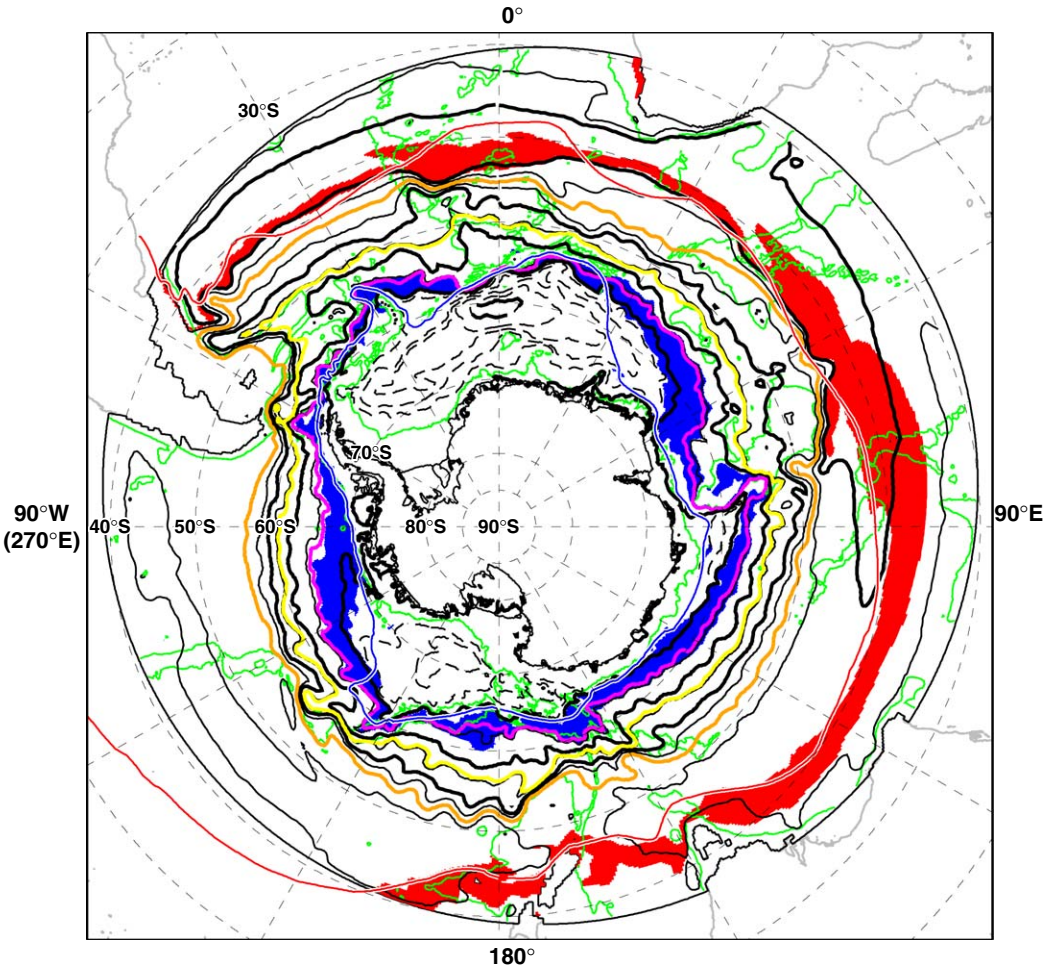

Figure 2. Modeled vertically integrated transport stream functions (annual mean). The interval of thin (thick) contours is 25 (50) Sv for positive values and 10 (50) Sv for negative values. Areas with dashed contours represent clockwise circulation. Red and blue areas (lines) indicate STF and Bdy in the model (inferred from observational data in *Orsi et al.* [1995]), respectively. Orange, yellow, and pink lines show m-SAF, m-PF, and m-SACCF (150, 70, and 20 Sv stream functions), respectively. Green contours indicate 3000 m isobath. Gray lines show coastline outside of the model domain.

of basal meltwater of each ice shelf group. The sum of all virtual tracers in the ocean corresponds to the total melting amount of all Antarctic ice shelves.

3. The Antarctic Circumpolar Current in the Model: Boundaries and Fronts

In this section, we evaluate the representations of the eastward flowing ACC, with a focus on the boundaries and fronts, to assess ocean circulation in this model. *Orsi et al.* [1995] described in detail ACC features from available hydrography data in the Southern Ocean. We compare the frontal systems of ACC between observation and model results. There are northern and southern boundaries of the ACC. The two boundaries are the Subtropical Front (STF) and southern boundary of the ACC (Bdy), which separate the ACC regime from the subtropical and subpolar regimes. These boundaries are defined by the water mass characteristics. The ACC vigorously flows eastward between the two boundaries and consists of multiple frontal jets. Some of these jets have circumpolar structures and are referred to as the Sub-Antarctic Front (SAF), the Polar Front (PF), and the Southern ACC front (SACCF), from north to south. The model used in this study can reasonably reproduce these ACC features as shown below.

Figure 2 shows the vertically integrated transport stream function and the ACC boundaries and fronts in this model. Note that the annual mean volume transport of the ACC across the Drake Passage is 174.2 Sv in this model. We define a modeled STF (m-STF) by a salinity range from 34.6 to 35.0 psu at 100 m depth (red

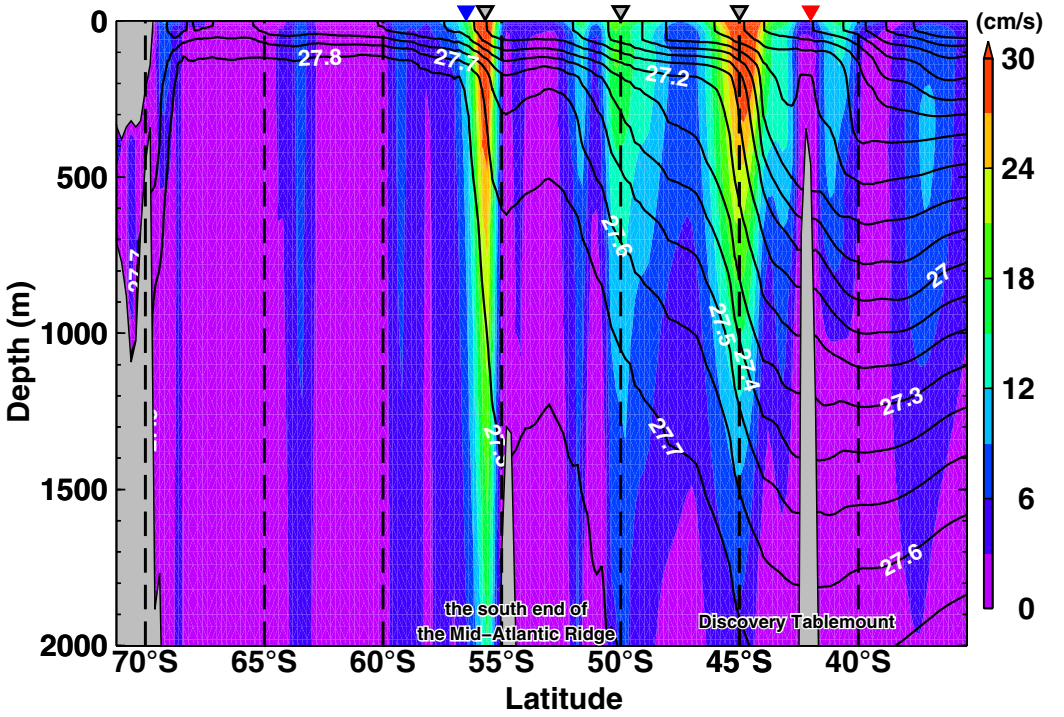

Figure 3. Vertical sections of the annual mean current magnitude (color) and potential density anomaly (contour with label) along the Greenwich Meridian. Red and blue inverted triangles indicate the positions of m-STF and m-Bdy, respectively (see text for the definitions). Gray inverted triangles show positions of deep-reaching currents along with steep density slope, corresponding to m-SAF, m-PF, and m-SACCF from north to south, respectively.

colored areas in Figure 2), following the definition of *Orsi et al.* [1995]. The m-STF extends eastward from the eastern side of the South American continent to 160°W (200°E) between 40°S and 50°S where this front leaves the model domain. The position of the m-STF is consistent with the STF distribution inferred from hydrographic data (red line in Figure 2) [*Orsi et al.*, 1995].

Bdy in the model (m-Bdy) is defined by a salinity range from 34.4 to 34.5 psu on the potential density surface of 27.6 kg m^{-3}. Although the distribution of the m-Bdy is largely consistent with observational estimates (blue line in Figure 2) [*Orsi et al.*, 1995], the eastern extents of the Weddell and Ross Gyres and the northern extent of the Kerguelen Gyre are slightly overestimated. The position of m-Bdy approximately corresponds to the zero line of the transport stream function, indicating that the boundary defined by the water mass is a good indicator of ocean flow regimes in this model. Large-scale anticyclonic/clockwise circulations (Weddell, Kerguelen, and Ross Gyres) exist south of the m-Bdy [*Gordon*, 2001]. The modeled volume transports of the Weddell, Kerguelen, and Ross Gyres are 54.5, 13.6, and 28.6 Sv, respectively. Note that the Weddell Gyre in this model has a single cell structure, although some previous observational and model studies showed a double cell structure [*Mosby*, 1934; *Beckmann et al.*, 1999; *Marsland and Wolff*, 2001]. Along the Antarctic continent, a westward flowing coastal current, which is driven by easterly winds, is produced south of the (m-)Bdy. In the marginal seas, the coastal current represents the southern limb of several large clockwise subpolar gyres.

Figure 3 shows vertical sections of current speed and the potential density anomaly along the Greenwich Meridian in the model. There are three deep-reaching jets between the m-STF and m-Bdy. The core of these jets reaches a depth of 1500 m and surface current speeds are 20–30 cm/s. These jets are accompanied by the rapid northward deepening of potential density surfaces (i.e., strongly sloped isopycnals). Along the Greenwich Meridian, these modeled fronts are located at latitudes of 45°S, 50°S, and 56°S (black triangles in Figure 3), corresponding to 150, 70, and 20 Sv of the transport stream lines, respectively (see corresponding orange, yellow, and pink lines in Figure 2). For convenience, we use these stream functions as m-SAF, m-PF, and m-SACCF. The front positions in the model are approximately consistent with those estimated from hydrographic indicators [see *Orsi et al.*, 1995, Figure 11].

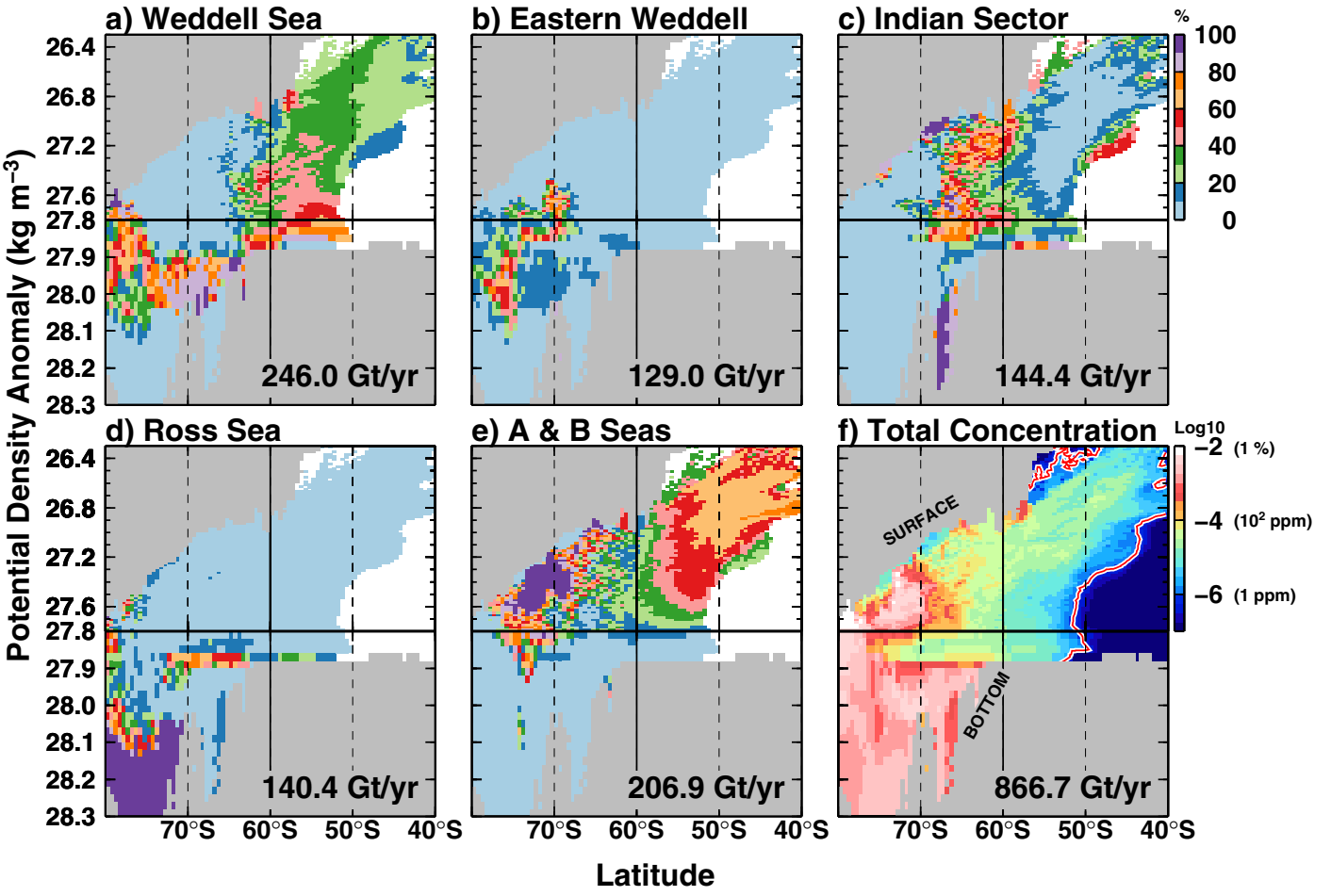

Figure 4. Vertical distribution of the zonal mean of basal meltwater tracers released from Antarctic ice shelf regions in the latitude-density domain at the end of integration. Note that the scaling of the vertical axis is different above and below the potential density anomaly of 27.8 kg m^{-3}. (a–e) The percentage of meltwater tracer of each ice shelf region to the total meltwater tracer in the Figure 4f. Vertical and horizontal axes indicate the potential density anomaly referenced to the surface and latitude, respectively. The area of the total tracer concentration smaller than 10^{-6} (red contours in the Figure 4f) is masked out in the Figures 4a–4e. The abbreviation "A & B Seas" indicates the Amundsen and Bellingshausen Seas.

4. Virtual Tracers of Basal Meltwater Released From Antarctic Ice Shelves

4.1. Vertical and Horizontal Distribution of Basal Meltwater Tracers

Figure 4f shows the circumpolar mean concentration of the total virtual tracers (i.e., basal meltwater released from all ice shelves) in the latitude-density domain at the end of the 10 year integration. The amount of the virtual tracers increases with time. There is a high concentration of tracers of approximately 1.5% in coastal regions; however, the basal meltwater amount is small compared to the total amount of ocean water. Observational results showed a few percent of ice shelf basal meltwater in coastal regions just off the ice shelf [*Jenkins*, 1999; *Jenkins and Jacobs*, 2008; *Jacobs et al.*, 2011; *Nakayama et al.*, 2013]. The high-concentration zones split into surface/subsurface and bottom layers south of 60°S. Focusing on the zone where the mean concentration is higher than 10 ppm (green in Figure 4f), the high-concentration zone extends up to 40°S in the surface/subsurface layer between 26.4 and 27.2 kg m^{-3} and extends to 50°S in the bottom layer denser than 27.8 kg m^{-3}.

Table 1. Total Basal Meltwater Distribution of Antarctic Ice Shelves[a]

		South (<60°S)	North (≥ 60°S)	Subtotal (Layer)
Upper	$\sigma_\theta < 27.8$ kg m^{-3}	281.8	68.4	350.2 (40%)
	$z < 1500$ m	584.5	82.6	667.1 (77%)
Lower	$\sigma_\theta \geq 27.8$ kg m^{-3}	455.9	60.6	516.5 (60%)
	$z \geq 1500$ m	153.2	46.4	199.6 (23%)
	Subtotal (Latitude)	737.5 (85 %)	129.0 (15 %)	866.7 (100%)

[a]The unit is Gt/yr. Numbers in parentheses indicate the percentage of the virtual tracer with respect to the total tracer amount (866.7 Gt/yr).

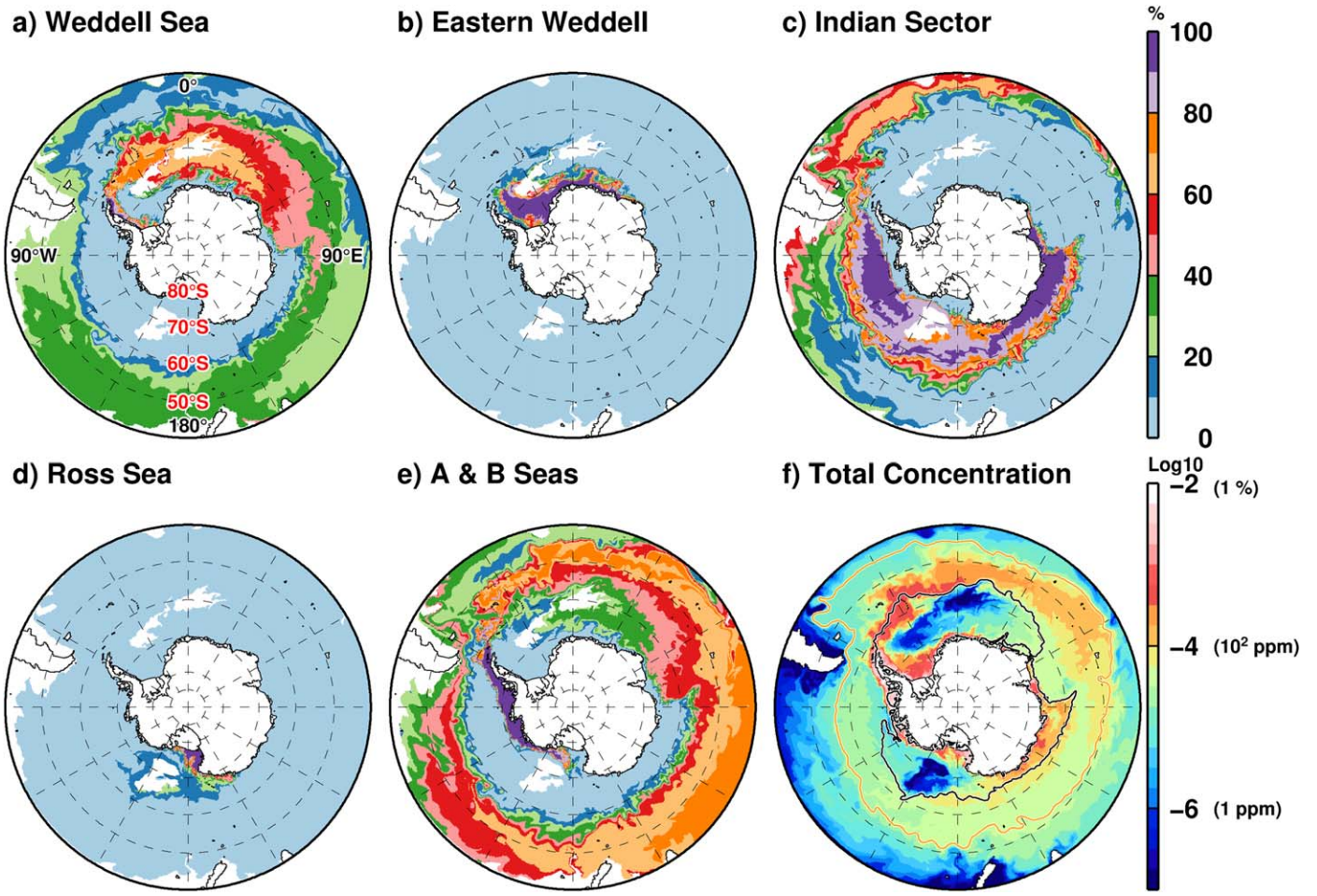

Figure 5. Horizontal distribution of basal meltwater tracers at the surface at the end of integration. (a–e) The percentage of the meltwater tracer of each ice shelf region to the total meltwater concentration in the Figure 5f. The area of the total tracer concentration smaller than 10^{-6} is masked out in the Figures 5a–5e. In the Figure 5f, the zero line of the transport stream function (as representatives of m-Bdy, black line) and m-SAF (orange line) are superimposed.

Here we show a quantitative distribution of the total basal meltwater from Antarctic ice shelves. The model domain is divided into four regions by latitude and depth/ocean density (Table 1). The basal meltwater is released at a total rate of 867 Gt/yr on average during the last 10 years. Since the virtual tracer is only released in the melting phase of the ice shelf base, the total amount of the meltwater tracer is larger than the net melting amount of 800 Gt/yr. Approximately 85% and 15% of the total meltwater tracer are supplied to regions south and north of 60°S, respectively. Vertically, approximately 77% and 23% of the total amount are supplied to layers above and below 1500 m depth, respectively. Roughly speaking, this result means that only a quarter of the basal meltwater is found in deep and bottom water masses.

Figure 5f shows the horizontal distribution of the total basal meltwater in the surface layer at the end of the integration. High-concentration regions of 10^3-10^4 ppm (red and pink colors in Figure 5f) are present around the Antarctic continent. High-concentration bands (>10 ppm) extend circumpolarly over the Southern Ocean. In particular, relatively high concentrations of up to about 10^3 ppm are observed in the northern part of the Weddell Gyre (approximately along the m-Bdy) and over the Australian-Antarctic Basin (south of the m-Bdy).

Figure 6f shows the horizontal distribution of the total basal meltwater in the bottom layer. Similar to the surface distribution, there are high-concentration regions of 10^2-10^4 ppm in the Antarctic coastal margins. The bottom concentration is strongly controlled by the bottom topography, because the ocean circulation, which distributes the tracer, is constrained by the topographic features like the mid-ocean ridges. A part of the basal meltwater tracer crosses the 3000 m depth contour and contributes to the bottom water.

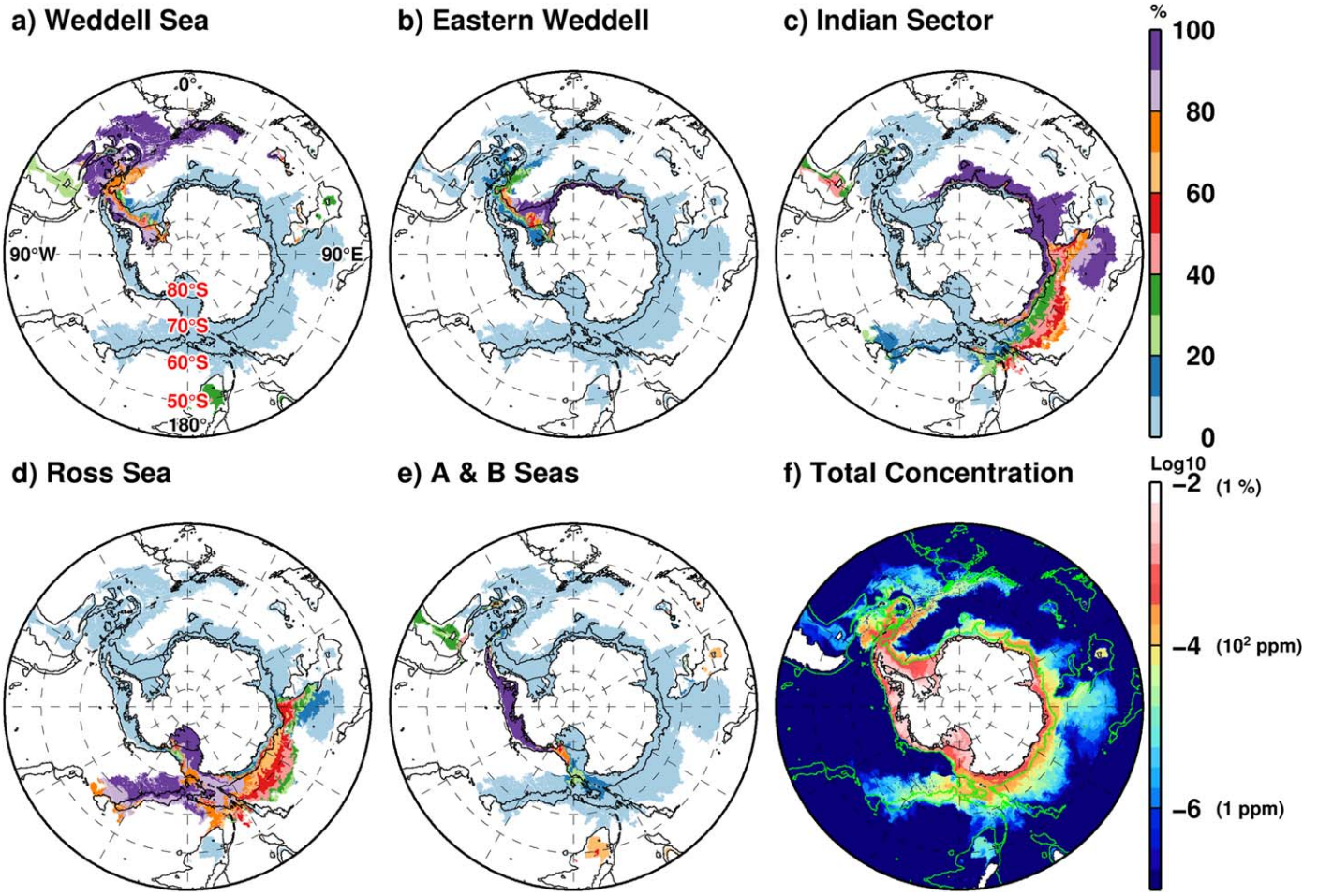

Figure 6. Same as Figure 5, but for the bottom. Black contours in (a–e) and green contours in (f) indicate 3000 m isobath.

High-concentration zones ($>10^2$ ppm) extend along the western side of large-scale cyclonic gyre circulations in the Weddell Sea, the Australian-Antarctic Basin, and the Ross Sea [*Gordon*, 2001, Figure 2]. These high-concentration regions (e.g., >10 ppm, green in Figure 6f) extend up to 50°S in the bottom layer along the eastern flank of the main ridges.

The bottom distribution of the basal meltwater is generally consistent with that of Antarctic Bottom Water (AABW) inferred from Chlorofluorocarbon (CFCs) [*Orsi et al*., 1999]. They agree well because both CFCs and basal meltwater are transported into the deeper layer through active dense water formation in the Antarctic coastal regions. The sea ice-ocean model with a horizontal resolution of approximately 10–20 km along the coastal margins enables this study to reproduce high sea ice production and dense water formation in Antarctic coastal polynyas to some extent [*Marsland et al*., 2004; *Kusahara et al*., 2010; *Kusahara and Hasumi*, 2013]. For example, broad high-concentration areas are detected across the continental rise and in further offshore regions in longitudinal ranges from 120°E to 150°E. This is consistent with the fact that there is active dense shelf water formation at coastal polynyas along the East Antarctic continental shelf [*Kusahara et al*., 2010].

4.2. Contributions of Meltwater of Each Ice Shelf Group

Basal meltwater released from Antarctic ice shelves widely spreads over the Southern Ocean, as shown in the previous subsection. In this subsection, we compare the regional ice shelf meltwater tracer to the total tracer amount (Figures 4a–4e, 5a–5e, and 6a–6e). The analysis below clearly shows the pathways of each ice shelf group's basal meltwater.

4.2.1. Ice Shelves in the Weddell Sea (Group A)

Basal meltwater released from ice shelves in the Weddell Sea (red ice shelves in Figure 1) accounts for approximately 80% of the total tracer amount south of 60°S in the potential density range between 27.6 and 28.1 kg m^{-3} (Figure 4a). This density range extends from surface to bottom over the continental shelf and slope regions in the Weddell Sea. At latitudes north of 60°S, the ratio of the basal meltwater from the Weddell Sea ice shelves is 30–40% in layers lighter than 27.8 kg m^{-3}.

In the surface layer, a large contribution of the Weddell Sea ice shelves tracer extends from the tip of the Antarctic Peninsula along the northern part of the Weddell Gyre (Figure 5a). Along the path of the eastward flowing ACC, this tracer accounts for 30–40% of the total tracer amount in the surface layer in the Indian sector and in the Ross, Amundsen, and Bellingshausen Seas (i.e., in the ACC regime between Bdy and STF).

In the bottom layer, the meltwater tracer from the Weddell Sea ice shelves has a pronounced impact on the concentration over the northern part of the Weddell Abyssal Plain (Figure 6a). This marked signal is observed along the eastern side of the Antarctic Peninsula and extends to the Scotia Sea (40°W, 57.5°S) and to the southern end of the Mid-Atlantic Ridge. A part of this tracer penetrates into the Argentine Basin in the Atlantic Ocean.

4.2.2. Eastern Weddell Ice Shelves (Group B)

A basal meltwater tracer released from the Eastern Weddell Ice Shelves (green ice shelves in Figure 1) is confined to the coastal regions south of 65°S and in the potential density range between 27.6 and 28.1 kg m^{-3} (Figure 4b). In the surface layer, the meltwater tracer is advected onto the inner Weddell shelf regions by the westward flowing coastal currents (Figure 5b) and accounts for a large part of the total tracer amount in the western and southern sides of the Weddell Gyre. There, the tracer of the ice shelf group B overweighs the local source of the ice shelf group A.

Similar to the surface distribution, the meltwater tracer at the bottom is also advected westward by coastal currents (Figure 6b). The signal splits into two branches at around 30°W. The southern branch extends southwestward to the Filchner Ice Shelf cavity along the coastline and grounding line. The other branch spreads westward along the continental slope (see 3000 m depth contour in Figure 6).

4.2.3. Ice Shelves in the Indian Sector (Group C)

There are many coastal polynyas at latitudes of approximately 68°S in East Antarctica [*Massom et al*., 1998]. High sea ice production at coastal polynyas leads to dense shelf water formation, which is a precursor of AABW [*Kusahara et al*., 2010]. The basal meltwater tracer released from ice shelves in the Indian sector (blue ice shelves in Figure 1) significantly contributes throughout the water column in latitude ranges from 70°S to 60°S. This indicates that the meltwater tracer is entrained in dense shelf waters that sink into the deep ocean (Figure 4c).

Horizontally, the tracer ratio in the surface layer over the Australian-Antarctic Basin is dominated by the meltwater tracer originating from the ice shelves of the Indian sector (Figure 5c). The signal extensively spreads eastward to the Bellingshausen Sea along the ACC and accounts for a significant fraction of the total amount in the regions deeper than 3000 m in the Ross, Amundsen, and Bellingshausen Seas. A part of the signal extends beyond the Drake Passage, reaching north of 50°S. The leading edge of the signal reaches the north of the Kerguelen Plateau, and takes approximately 10 years to encircle the Southern Ocean.

At the bottom, the meltwater tracer spreads to the southern part of the Australian-Antarctic Basin and to the continental slope and rise regions of the Enderby Abyssal Plain (Figure 6c). The signal is concentrated on the eastern flank of the Kerguelen Plateau, reflecting northward deep western boundary currents [*Fukamachi et al*., 2010]. On the western side of the Kerguelen Plateau, there is also a large contribution region of this tracer, consistent with AABW formation around Cape Darnley [*Ohshima et al*., 2013]. At longitudes around the Greenwich Meridian, there are high contributions of the signal approximately along the 3000 m depth contour, which is representative of the continental slope and rise. This indicates that the meltwater tracer is entrained in dense waters sinking into deep ocean, and it is transported to the Weddell Abyssal Plain by westward flowing coastal currents.

4.2.4. Ice Shelves in the Ross Sea (Group D)

The basal meltwater released from ice shelves in the Ross Sea (yellow ice shelves in Figure 1) dominates the concentration of tracers south of 70°S and in the lower layer denser than 28.0 kg m^{-3}

Table 2. Constituents of Basal Meltwater of Antarctic Ice Shelves at the Surface/Subsurface Layer North of 60°S[a]

Location of Ice Shelves	Group	$\sigma_\theta < 27.8$ kg m^{-3}	z < 1500 m
Weddell Sea	A	25.3	35.0
Eastern Weddell	B	1.6	2.3
Indian sector	C	10.2	12.3
Ross Sea	D	0.2	0.2
A & B Seas	E	31.1	32.8
North (≥ 60°S)	All	68.4	82.6

[a]The unit is Gt/yr. The abbreviation "A & B Seas" indicates the Amundsen and Bellingshausen Seas.

(Figure 4d). At the surface, large contribution regions are mainly observed in the western Ross Sea. A part of the meltwater signal extends westward along the coastline to 150°E (Figure 5d).

Similar to the surface distribution, large contributions at the bottom are observed over the Ross continental shelf region (Figure 6d). Since there are active coastal polynyas in front of the Ross Ice Shelf in winter [*Tamura et al.*, 2008; *Drucker et al.*, 2011], the meltwater tracer locally penetrates into lower layers [*Kusahara and Hasumi*, 2013]. The bottom signals split into two branches. The eastern branch extends northeastward along the southern flank of the Pacific-Antarctic Ridge. From this branch, a part of the meltwater tracer leaks into the Southwest Pacific Basin and the Tasman Abyssal Plain, while the other branch extends westward to the Australian-Antarctic Basin along the continental slope and rise.

4.2.5. Ice Shelves in the Amundsen and Bellingshausen Seas (Group E)

The basal meltwater released from ice shelves in the Amundsen and Bellingshausen Seas (orange ice shelves in Figure 1) significantly contributes to the total concentration at latitudes between 75°S and 40°S and in the surface/subsurface layer (Figure 4f). Horizontally, the meltwater tracer dominates the shallow continental shelf and upper slope regions in the Amundsen and Bellingshausen Seas. Although a small part of the meltwater tracer is transported to the Ross Sea continental shelf region by westward coastal currents, most of this tracer is advected eastward by the ACC. Note that the westward coastal current has a surface-intensified structure, which is associated with a coastal density front. In the Amundsen and Bellingshausen Seas, the path of the ACC is geographically very adjacent to the ice shelves (Figure 2). The basal meltwater passing the Drake Passage spreads northward across the Scotia Sea via South Georgia Island and the signal extensively spreads eastward along the ACC (Figure 5e). A high-concentration ratio of more than 60% is observed circumpolarly north of 50°S. The meltwater tracer from ice shelves in the Amundsen and Bellingshausen Seas accounts for more than 40% of the total meltwater north of 60°S (Table 2).

This basal meltwater signal is confined to the regions shallower than 3000 m, because there is no significant dense water formation in coastal regions in the eastern Pacific sector. The meltwater advected onto the Ross Sea continental shelf penetrates into the lower layer because of high sea ice production at the front of the Ross Ice Shelf. The tracer at the bottom accounts for 20–40% of the total tracer over the Ross Sea continental shelf regions (Figure 6e).

5. Impacts on the Southern Ocean System

In the previous section, we have traced the pathway of basal meltwaters released from each ice shelf group. *Hellmer* [2004] showed that the basal meltwater of Antarctic ice shelves has a large impact on sea ice and deep ocean thermohaline circulation fields in the Southern Ocean. However, it is not clear how much the basal meltwater released from regional ice shelves have influenced these fields. In this section, we perform a series of numerical experiments, in which the thermodynamic interaction under a specific ice shelf group is turned off, and investigate the impact of basal meltwater from specified ice shelves on sea ice and deep thermohaline circulation. The NOWDL (NOEWD/NOIND/NORSS/NOABS) case is a numerical experiment neglecting thermodynamic interaction under ice shelves in the Weddell Sea (Eastern Weddell Sea/Indian sector/Ross Sea/Amundsen-Bellingshausen Seas). A numerical experiment without the thermodynamic interaction under all the ice shelves is also performed (NOTHM case). In all cases, the initial condition is taken from the end of the fifteenth year in the standard experiment (CTRL case), and a 10 year integration (i.e., 16th–25th year) is performed for each case. The model results averaged over the last 3 years are used for the following analyses. Since the model is repeatedly driven by the same climatological surface forcing during the integration, the interannual variability is small and thus the averaging period of the 3 years is sufficient to represent mean fields in each experiment.

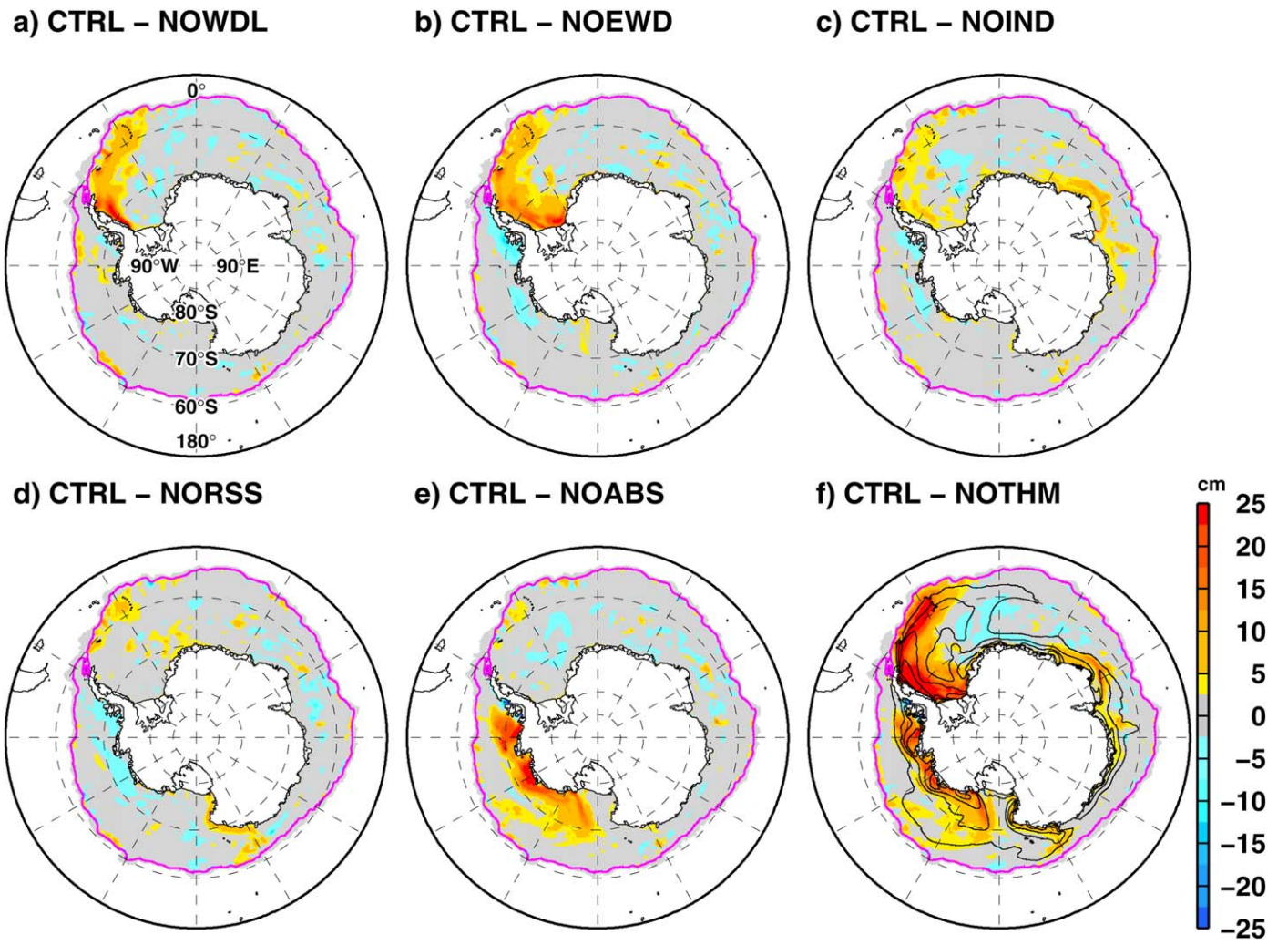

Figure 7. Horizontal distribution of the sea ice thickness anomaly in September. Result in the CTRL case is removed from those in the experiments. The pink line in each plot indicates the CTRL sea ice edge defined by a sea ice concentration of 15%. In the (f), monthly mean thickness in the CTRL case is overlaid with a contour interval of 50 cm (black contour). Areas of magnitude difference smaller than 2.5 cm are shaded gray to highlight areas of large change.

5.1. Sea Ice

The modeled sea ice thickness in winter is generally consistent with the observational estimate of *Worby et al*. [2008] (see the contours of sea ice thickness in Figure 7f). In this model, there are no discernable differences in the sea ice extent between the CTRL and NOTHM cases, although *Bintanja et al*. [2013] suggested that basal meltwater of Antarctic ice shelves causes sea ice expansion. We do find pronounced differences in sea ice thickness in our model. The sea ice in the CTRL case is thicker than that in the NOTHM case at some places and reaches a maximum difference of 25 cm (Figure 7f). The areas of large differences approximately correspond to pathways of basal meltwaters at the surface (Figure 5). The existence of the basal meltwater from Antarctic ice shelves stabilizes the ocean surface layer, and thus, sea ice is effectively formed without entraining relatively warm subsurface waters. The most pronounced differences of sea ice thickness are present in the western and northwestern sides of the Weddell Gyre and over coastal regions of the Amundsen and Bellingshausen Seas. The basal meltwater released from ice shelves in the Weddell and Eastern Weddell Seas profoundly affects sea ice thickness distributions along the eastern side of the Antarctic Peninsula (Figures 7a and 7b). The basal meltwater from ice shelves in the Amundsen and Bellingshausen Seas can modify the sea ice thickness in the coastal regions locally (Figure 7e).

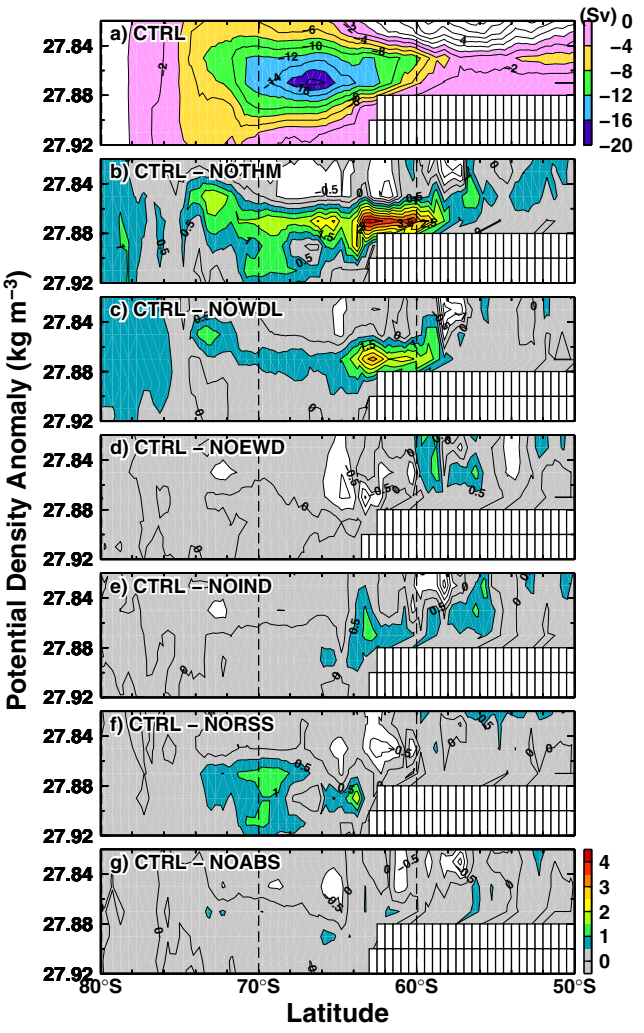

Figure 8. (a) Stream function of zonally integrated, annual-mean meridional overturning circulation in the latitude-density domain, and (b–g) anomalies of the numerical experiments (see text for the detail). Negative values of the stream function in the Figure 8a indicate anticlockwise circulation. Positive values of the anomaly in the lower plots (i.e., CTRL—NOTHM) indicate that the AABW cell in the experiment (NOTHM case) is stronger than that in the CTRL case. White blocks indicate no water in the density class. Areas of magnitude differences smaller than 0.5 Sv are shaded gray to highlight areas of large change.

5.2. Deep Ocean Thermohaline Circulation

Sinking dense waters from the Antarctic coastal regions to the deep Southern Ocean along continental slopes constitute the lower limb of the meridional overturning in the Southern Hemisphere. In this subsection, we term the overturning circulation cell formed at the bottom "AABW cell" [see also *Kusahara and Hasumi*, 2013, Figure 13]. The magnitude (absolute value) of the AABW cell in the CTRL case is smaller than that in the NOTHM case (Figure 8b). This result indicates that the basal meltwater released from ice shelves weakens the AABW cell [*Hellmer*, 2004; *Kusahara and Hasumi*, 2013]. The basal meltwaters of the ice shelves in the Weddell and Ross Seas play a role in weakening the AABW cell (Figures 8c and 8f), followed by those in the Eastern Weddell Sea and the Indian sector to some extent (Figures 8e and 8d). The basal meltwaters of these ice shelves experience high sea ice formation in the coastal areas (i.e., coastal polynyas) in winter, and thus, a part of the meltwater is transported into the bottom layer through deep convection at Antarctic coastal margins. Therefore, these meltwaters influence the magnitude of the AABW cell. In contrast, since the basal meltwaters of ice shelves in the Amundsen and Bellingshausen Seas are confined to the surface and subsurface layers (Figure 4e), the meltwater negligibly affects the AABW cell.

6. Summary and Discussion

We have investigated spreading pathways of basal meltwater released from Antarctic ice shelves by tracing virtual tracers in a circumpolar coupled ice shelf-sea ice-ocean model. We confirmed that the model can reproduce important features of the large-scale ocean circulations in the Southern Ocean, such as the ACC and subpolar gyres (Figures 2 and 3). The basal meltwater signal splits into the surface/subsurface and bottom layers as it travels to lower latitudes (Figure 4 and Table 1). The pathways of the meltwater tracers depend on formation site (Figures 5 and 6). The meltwater is advected from the formation site to other areas (i.e., downstream regions) by ambient ocean circulation. The basal meltwaters originating from ice shelves in the Weddell Sea, the Indian sector, and the Amundsen and Bellingshausen Seas are transported by the eastward flowing ACC and are distributed widely over the entire Southern Ocean (Figure 5 and Table 2). In particular, the meltwater tracer from ice shelves in the Amundsen, Bellingshausen, and Weddell Seas is effectively transported to lower latitudes north of 60°S after passing the Drake Passage (Figures 5a, 5c, and 5e and Table 2).

About a quarter of the meltwater tracer penetrates into the bottom layer through active dense water formation along Antarctic coastal margins (Table 1). The signal at the bottom spreads along the mid-ocean ridge system (Figure 6f), and the horizontal distribution in this model is generally consistent with that of the AABW inferred from the observed CFCs distribution [*Orsi et al*., 1999]. This is due to the fact that as well as the CFCs the basal meltwater experiences active dense water formation in coastal margins and is thereby transported from the surface to the seafloor. The basal meltwater from ice shelves in the Weddell and Ross Seas and in the Indian sector primarily accounts for the bottom concentration (Figures 4 and 6).

We have performed a series of numerical experiments in which the thermodynamic interaction under ice shelves is turned off regionally or completely. It is confirmed that the regional basal meltwaters impact sea ice and/or deep thermohaline circulation (Figures 7 and 8). Since basal meltwater of ice shelves influences sea ice fields, the basal meltwater might induce some feedback processes between atmosphere and sea ice/ocean. However, we can not assess such feedback effects by the model without an interactive atmospheric component. Sea ice extent is strongly controlled by atmospheric conditions, which may partly or fully explain why no pronounced change in sea ice extent is found in our numerical experiments forced by prescribed atmosphere.

The observed meltwater concentration (sometimes referred to as "meltwater fraction") is estimated by the mixing ratio among the pure basal meltwater of ice shelves and ambient water masses (e.g., Circumpolar Deep Water), combined with properties of tracers, such as temperature, salinity, helium, neon, and oxygen. Meltwater concentrations have been calculated in limited areas adjacent to ice shelf fronts in the Amundsen and Bellingshausen Seas [*Jenkins*, 1999; *Jenkins and Jacobs*, 2008; *Jacobs et al*., 2011; *Nakayama et al*., 2013], the Weddell Sea [*Schlosser*, 1986; *Schlosser et al*., 1990; *Weppernig et al*., 1996; *Huhn et al*., 2008], and the Ross Sea [*Loose et al*., 2009]. However, there has so far been no study that shows the observed meltwater concentration over the entire Southern Ocean. At this point of time, therefore, it is not possible to circumpolarly validate the modeled meltwater concentration in this study (Figures 4f, 5f, and 6f) against observations. Moreover, although origins of the basal meltwater of ice shelves are identified in this model, it seems to be impossible to discern the origins of the basal meltwater based on observation data because the tracer properties of ice shelf basal meltwater are considered to be nearly uniform among Antarctic ice shelves. However, the numerical model results in this study are useful to discuss changes of water masses in the Southern Ocean in recent decades.

Helm et al. [2010] revealed that ocean salinity changes in the subsurface layers of the Southern Ocean between 1970 and 2005 can not be solely explained by increases of precipitation-minus-evaporation in recent decades. They suggest that an additional freshwater source originating from Antarctic ice sheets is required to induce the observed salinity change. They estimated that the required amount corresponds to approximately 0.5% of the mass of existing Antarctic ice shelves. There is no significant change of the number of small icebergs ($<$2–3 km in length) in recent years [*Tournadre et al*., 2012], although the Antarctic Ice Sheet has experienced calving events of large tabular icebergs [*Scambos et al*., 2000; *Long et al*., 2002; *Legresy et al*., 2010]. On the other hand, basal melting at the West Antarctic Ice Shelves has been reported to be more active in recent decades [*Jenkins et al*., 2010; *Jacobs et al*., 2011; *Pritchard et al*., 2012], and *Rignot et al*. [2013] and *Depoorter et al*. [2013] showed that the basal melting of Antarctic ice shelves accounts for larger fraction of the Antarctic Ice Sheet discharges than previously estimated. These facts suggest that the basal melting of ice shelves is or is becoming the dominant ablation process for Antarctic ice shelves. A portion of the basal meltwater of the Antarctic ice shelves is effectively transported to lower latitudes as shown in this study and therefore the basal meltwater could contribute to the salinity field at the surface/subsurface over the Southern Ocean, as well as melting icebergs in lower latitudes.

Ocean modeling studies that include an ice shelf component have commonly showed that atmospheric changes over the Southern Ocean lead to a pronounced enhancement of ice shelf basal melting [*Hellmer et al*., 2012; *Kusahara and Hasumi*, 2013; *Timmermann and Hellmer*, 2013]. These studies suggest that an increase of the basal meltwater of ice shelves could cause further freshening in the surface/subsurface and bottom layers over the Southern Ocean during the next hundred years. Since the response of basal melting to future climate changes is believed to be significantly different from one ice shelf to another [*Hellmer et al*., 2012; *Kusahara and Hasumi*, 2013; *Timmermann and Hellmer*, 2013] and the pathway of the meltwater depends on the formation site, the consequent freshening of the Southern Ocean is expected to be nonuniform in space. A better understanding of the Southern Ocean and Antarctic climate systems requires continuous monitoring of the Antarctic cryosphere changes and further improvement of existing climate models.

Acknowledgments
Numerical simulations were performed on a Fujitsu FX10 at the Information Technology Center, the University of Tokyo. This study was supported by Grant-in-Aids for Scientific Research A (26247080), B (23340138), and Research Activity Start-up (25887001) for the Japan Society for Promotion of Science (JSPS), by the Canon Foundation, and partly by the Sasagawa Scientific Research grant from the Japan Science Society. We are grateful to Dr. Ralph Timmermann and the two anonymous reviewers for their careful reading and constructive comments on the manuscript.

References

Aoki, S., S. R. Rintoul, S. Ushio, S. Watanabe, and N. L. Bindoff (2005), Freshening of the Adélie Land Bottom Water near 140°E, *Geophys. Res. Lett.*, *32*, L23601, doi:10.1029/2005GL024246.

Beckmann, A., H. H. Hellmer, and R. Timmermann (1999), A numerical model of the Weddell Sea: Large-scale circulation and water mass distribution, *J. Geophys. Res.*, *104*(C10), 23,375–23,391.

Bintanja, R., J. van Oldenborgh, S. S. Drijfhout, B. Wouters, and C. A. Katsman (2013), Important role for ocean warming and increased ice-shelf melt in Antarctic sea-ice expansion, *Nat. Geosci.*, *6*, 376–379, doi:10.1038/ngeo1767.

Boyer, T. P., S. Levitus, J. I. Antonov, R. A. Locarnini, and H. E. Garcia (2005), Linear trends in salinity for the World Ocean, 1955–1998, *Geophys. Res. Lett.*, *32*, L01604, doi:10.1029/2004GL021791.

Chelton, D. B., R. A. deSzoeke, M. G. Schlax, K. L. Naggar, and N. Siwertz (1998), Geographical variability of the first baroclinic Rossby Radius of deformation, *J. Phys. Oceanogr.*, *28*, 433–460.

Conkright, M. E., et al. (1998), World Ocean Database 1998 Documentation and Quality Control, Natl. Oceanogr. Data Cent., Silver Spring, Md.

Depoorter, M. A., J. L. Bamber, J. A. Griggs, J. T. M. Lenaerts, S. R. M. Ligtenberg, M. R. van den Broke, and G. Moholdt (2013), Calving fluxes and basal melt rates of Antarctic ice shelves, *Nature*, *502*, 89–92, doi:10.1038/nature12567.

Drucker, R., S. Martin, and R. Kwok (2011), Sea ice production and export from coastal polynyas in the Weddell and Ross Seas, *Geophys. Res. Lett.*, *38*, L17502, doi:10.1029/2011GL048668.

Dupont, T. K., and R. B. Alley (2005), Assessment of the importance of ice-shelf buttressing to ice-sheet flow, *Geophys. Res. Lett.*, *32*, L04503, doi:10.1029/2004GL022024.

Fukamachi, Y., S. R. Rintoul, J. A. Church, S. Aoki, S. Sokolov, M. A. Rosenberg, and M. Wakatsuchi (2010), Strong export of Antarctic Bottom Water east of the Kerguelen plateau, *Nat. Geosci.*, *3*, 327–331, doi:10.1038/NGEO842.

Gent, P. R., J. Willbrand, T. J. McDougall, and J. C. McWilliams (1995), Parameterizing eddy-induced tracer transports in ocean circulation models, *J. Phys. Oceanogr.*, *25*, 463–474.

Gladstone, R. M., G. R. Bigg, and K. W. Nicholls (2001), Iceberg trajectory modeling and meltwater injection in the Southern Ocean, *J. Geophys. Res.*, *106*(C9), 19,903–19,915.

Gordon, A. L. (2001), Current systems in the Southern Ocean, in *Encyclopedia of Ocean Sciences*, pp. 735–743, Academic Press, doi:10.1006/rwos.2001.0369.

Hellmer, H. H. (2004), Impact of Antarctic ice shelf basal melting on sea ice and deep ocean properties, *Geophys. Res. Lett.*, *31*, L10307, doi:10.1029/2004GL019506.

Hellmer, H. H., and S. S. Jacobs (1994), Temporal changes in shelf water of the southern Ross Sea, *Antarct. J. U. S.*, *29*(5), 123–124.

Hellmer, H. H., and D. J. Olbers (1989), A two-dimensional model for the thermohaline circulation under an ice shelf, *Antarct. Sci.*, *1*, 325–336.

Hellmer, H. H., O. Huhn, D. Gomis, and R. Timmermann (2011), On the freshening of the northwestern Weddell Sea continental shelf, *Ocean Sci.*, *7*, 305–316, doi:10.5194/os-7–305-2011.

Hellmer, H. H., F. Kauker, R. Timmermann, J. Determann, and J. Rae (2012), Twenty-first-century warming of a large Antarctic ice-shelf cavity by a redirected coastal current, *Nature*, *485*, 225–228, doi:10.1038/nature11064.

Helm, K. P., N. L. Bindoff, and J. A. Church (2010), Changes in the global hydrological-cycle inferred from ocean salinity, *Geophys. Res. Lett.*, *37*, L18701, doi:10.1029/2010GL044222.

Holland, D. M., and A. Jenkins (1999), Modeling thermodynamic ice-ocean interactions at the base of an ice shelf, *J. Phys. Oceanogr.*, *29*, 1787–1800.

Hooke, R. L. (2005), *Principles of Glacier Mechanics*, 429 pp., Cambridge Univ. Press, N. Y.

Huhn, O., H. H. Hellmer, M. Rhein, C. Rodehacke, W. Roether, M. P. Schodlok, and M. Schröder (2008), Evidence of deep- and bottom-water formation in the western Weddell Sea, *Deep Sea Res., Part II*, *55*, 1098–1116.

Huhn, O., M. Rhein, M. Hoppema, and S. van Heuven (2013), Decline of deep and bottom water ventilation and slowing down of anthropogenic carbon storage in the Weddell Sea, 1984–2011, *Deep Sea Res., Part I*, *176*, 66–84, doi:10.1016/j.dsr.2013.01.005.

Jacobs, S. S. (2004), Bottom water production and its links with the thermohaline circulation, *Antarct. Sci.*, *16*(4), 427–437, doi:10.1017/S095410200400224X.

Jacobs, S. S., and C. F. Giulivi (2010), Large multidecadal salinity trends near the Pacific-Antarctic continental margin, *J. Clim.*, *23*, 4508–4524, doi:10.1175/2010JCLI3284.1.

Jacobs, S. S., H. H. Hellmer, C. S. M. Doake, A. Jenkins, and R. M. Frolich (1992), Melting of ice shelves and the mass balance of Antarctica, *J. Glaciol.*, *38*, 375–387.

Jacobs, S. S., H. H. Hellmer, and A. Jenkins (1996), Antarctic ice sheet melting in the Southeast Pacific, *Geophys. Res. Lett.*, *23*(9), 957–960.

Jacobs, S. S., C. F. Giulivi, and P. A. Mele (2002), Freshening of the Ross Sea during the late 20th century, *Science*, *297*, 386–389, doi:10.1126/science.1069574.

Jacobs, S. S., A. Jenkins, C. F. Giulivi, and P. Dutrieux (2011), Stronger ocean circulation and increased melting under Pine Island Glacier ice shelf, *Nat. Geosci.*, *4*, 519–523, doi:10.1038/NGEO1188.

Jenkins, A. (1999), The impact of melting ice on ocean waters, *J. Phys. Oceanogr.*, *29*, 2370–2381.

Jenkins, A., and S. Jacobs (2008), Circulation and melting beneath George VI Ice Shelf, Antarctica, *J. Geophys. Res.*, *113*, C04013, doi:10.1029/2007JC004449.

Jenkins, A., P. Dutrieux, S. S. Jacobs, S. D. McPhail, J. R. Perrett, A. T. Webb, and D. White (2010), Observations beneath Pine Island Glacier in West Antarctica and implications for its retreat, *Nat. Geosci.*, *3*, 468–472, doi:10.1038/NGEO890.

Jongma, J. I., E. Driesschaert, T. Fichefet, H. Goosse, and H. Renssen (2009), The effect of dynamic-thermodynamic icebergs on the Southern Ocean climate in a three-dimensional model, *Ocean Modell.*, *26*, 104–113, doi:10.1016/j.ocemod.2008.09.007.

Kusahara, K., and H. Hasumi (2013), Modeling Antarctic ice shelf responses to future climate changes and impacts on the ocean, *J. Geophys. Res. Oceans*, *118*, 2454–2475, doi:10.1002/jgrc.20166.

Kusahara, K., H. Hasumi, and T. Tamura (2010), Modeling sea ice production and dense shelf water formation in coastal polynyas around East Antarctica, *J. Geophys. Res.*, *115*, C10006, doi:10.1029/2010JC006133.

Kusahara, K., H. Hasumi, and G. D. Williams (2011), Dense shelf water formation and brine-driven circulation in the Adélie and George V Land region, *Ocean Modell.*, *37*, 122–138, doi:10.1016/j.ocemod.2011.01.008.

Legresy, B., et al. (2010), Crack in the Mertz Glacier, Antarctica, technical report, Antarct. *Clim. and Ecosyst. Coop. Res. Cent.*, Hobart, Tasmania.

Leonard, B. P., M. K. MacVean, and A. P. Lock (1993), Positivity-preserving numerical schemes for multidimensional advection, *Tech. Memo 106005*, 62 pp.

Long, D. G., J. Ballantyne, and C. Bertoia (2002), Is the number of Antarctic icebergs really inreasing?, *Eos Trans. AGU*, *83*(42), 469–480.
Loose, B., P. Schlosser, W. M. Smethie, and S. Jacobs (2009), An optimized estimate of glacial melt from the Ross Ice Shelf using noble gases, stable isotopes, and CFC transient tracers, *J. Geophys. Res.*, *114*, C08007, doi:10.1029/2008JC005048.
Marsland, S. J., and J. O. Wolff (2001), On the sensitivity of Southern Ocean sea ice to the surface freshwater flux: A model study, *J. Geophys. Res.*, *106*(C2), 2723–2741.
Marsland, S. J., N. L. Bindoff, G. D. Williams, and W. F. Budd (2004), Modeling water mass formation in the Mertz Glacier Polynya and Adélie Depression, East Antarctica, *J. Geophys. Res.*, *109*, C11003, doi:10.1029/2004JC002441.
Martin, T., and A. Adcroft (2010), Parameterizing the fresh-water flux from land ice to ocean with interactive icebergs in a coupled climated model, *Ocean Modell.*, *34*, 111–124, doi:10.1016/j.ocemod.2010.05.001.
Massom, R. A., P. T. Harris, K. J. Michael, and M. J. Potter (1998), The distribution and formative processes of latent-heat polynyas in East Antarctica, *Ann. Glaciol.*, *27*, 420–426.
Mosby, H. (1934), The water of the Atlantic Ocean, in *Scientific Results of the Norwegian Antarctic Expedition 1927–1928*, vol. 11, 131 pp., Oslo, Norway.
Nakayama, Y., M. Schröder, and H. H. Hellmer (2013), From circumpolar deep water to the glacial meltwater plume on the eastern Amundsen Shelf, *Deep Sea Res., Part I*, *77*, 50–62, doi:10.1016/j.dsr.2013.04.001.
Noh, Y., and H. J. Kim (1999), Simulations of temperature and turbulence structure of the oceanic boundary layer with the improved near-surface process, *J. Geophys. Res.*, *104*(C7), 15,621–15,634.
Ohshima, K. I., et al. (2013), Antarctic Bottom Water production by intense sea-ice formation in the Cape Darnley polynya, *Nat. Geosci.*, *6*, 235–240, doi:10.1038/NGEO1738.
Orsi, A. H., T. Whiteworth III, and W. D. Nowlin Jr. (1995), On the meridional extent and fronts of the Antarctic Circumpolar Current, *Deep Sea Res., Part I*, *42*(5), 641–673.
Orsi, A. H., G. C. Johnson, and J. L. Bullister (1999), Circulation, mixing, and production of Antarctic Bottom Water, *Prog. Oceanogr.*, *43*, 55–109.
Pritchard, H. D., R. J. Arthern, D. G. Vaughan, and L. A. Edwards (2009), Extensitve dynamic thinning on the margins of the Greenland and Antarctic ice sheets, *Nature*, *461*, 971–975, doi:10.1038/nature08471.
Pritchard, H. D., S. R. M. Ligtenberg, H. A. Fricker, D. G. Vaughan, M. R. van den Broeke, and L. Padman (2012), Antarctic ice-sheet loss driven by basal melting of ice shelves, *Nature*, *484*, 502–505, doi:10.1038/nature10968.
Rignot, E., J. L. Bamber, M. R. van den Broeke, C. Davis, Y. Li, W. J. van de Berg, and E. V. Meijgaard (2008), Recent Antarctic ice mass loss from radar interferometry and regional climate modelling, *Nat. Geosci.*, *1*, 106–110, doi:10.1038/ngeo102.
Rignot, E., I. Velicogna, M. R. van den Broeke, A. Monaghan, and J. T. M. Lenaerts (2011), Acceleration of the contribuion of the Greenland and Antarctic ice sheets to sea level rise, *Geophys. Res. Lett.*, *38*, L05503, doi:10.1029/2011GL046583.
Rignot, E., S. S. Jacobs, J. Mouginot, and B. Scheuchl (2013), Ice shelf melting around Antarctica, *Science*, *341*, 266–270, doi:10.1126/science.1235798.
Rintoul, S. R. (2007), Rapid freshening of Antarctic Bottom Water formed in the Indian and Pacific oceans, *Geophys. Res. Lett.*, *34*, L06606, doi:10.1029/2006GL028550.
Rodehacke, C. B., H. H. Hellmer, O. Huhn, and A. Beckmann (2007), Ocean/ice shelf interaction in the southern Weddell Sea: Results of a regional numerical helium/neon simulation, *Ocean Dyn.*, *57*, 1–11, doi:10.1007/s10236-006-0073-2.
Röske, F. (2006), A global heat and freshwater forcing dataset for ocean models, *Ocean Modell.*, *11*, 235–297, doi:10.1016/j.ocemod.2004.12.005.
Scambos, T. A., C. Hulbe, M. Fahnestock, and J. Bohlander (2000), The link between climate warming and break-up of ice shelves in the Antarctic Peninsula, *J. Glaciol.*, *46*(154), 516–530.
Schlosser, P. (1986), Helium: A new tracer in Antarctic oceanography, *Nature*, *321*(15), 233–235.
Schlosser, P., R. Bayer, A. Foldvik, T. Gammerlsrød, G. Rohardt, and K. O. Münnich (1990), Oxygen 18 and Helium as tracers of Ice Shelf Water and water/ice interaction in the Weddell Sea, *J. Geophys. Res.*, *95*(C3), 3253–3263.
Schoof, C. (2007), Ice sheet grounding line dynamics: Steady states, stability, and hysteresis, *J. Geophys. Res*, *112*, F03S28, doi:10.1029/2006JF000664.
Shepherd, A., D. Wingham, and E. Rignot (2004), Warm ocean is eroding West Antarctic Ice Sheet, *Geophys. Res. Lett.*, *31*, L23402, doi:10.1029/2004GL021106.
Shimada, K., S. Aoki, K. I. Ohshima, and R. Rintoul (2012), Influence of Ross Sea Bottom Water changes on the warming and freshening of the Antarctic Bottom Water in the Australian-Antarctic Basin, *Ocean Sci.*, *8*, 419–432, doi:10.5194/os-8–419-2012.
Silva, T. A. M., G. R. Bigg, and K. W. Nicholls (2006), Contribution of giant icebergs to the Southern Ocean freshwater flux, *J. Geophys. Res.*, *111*, C03004, doi:10.1029/2004JC002843.
Tamura, T., K. I. Ohshima, and S. Nihashi (2008), Mapping of sea ice production for Antarctic coastal polynyas, *Geophys. Res. Lett.*, *35*, L07606, doi:10.1029/2007GL032903.
Timmermann, R., and H. H. Hellmer (2013), Southern Ocean warming and increased ice shelf basal melting in the twenty-first and twenty-second centuries based on coupled ice-ocean finite-element modelling, *Ocean Dyn.*, *63*, 1011–1026.
Timmermann, R., et al. (2010), A consistent data set of Antarctic ice sheet topography, cavity geometry, and global bathymetry, *Earth Syst. Sci. Data*, *2*, 261–273, doi:10.5194/essd-2–261-2010.
Timmermann, R., Q. Wang, and H. H. Hellmer (2012), Ice-shelf basal melting in a global finite-element sea-ice/ice-shelf/ocean model, *Ann. Glaciol.*, *53*, 303–314, doi:10.3189/2012AoG60A156.
Tournadre, J., K. Whitmer, and F. Girard-Ardhuin (2008), Iceberg detection in open water by altimeter waveform analysis, *J. Geophys. Res.*, *113*, C08040, doi:10.1029/2007JC004587.
Tournadre, J., F. Girard-Ardhuin, and B. Legrésy (2012), Antarctic icebergs distributions, 2002–2010, *J. Geophys. Res.*, *117*, C05004, doi:10.1029/2011JC007441.
Weppernig, R., P. Schlosser, S. Khatiwala, and R. G. Fairbanks (1996), Isotope data from Ice Station Weddell: Implications for deep water formation in the Weddell Sea, *J. Geophys. Res.*, *101*(C11), 25,723–25,739.
Worby, A. P., C. A. Geiger, M. J. Paget, M. L. Van Woert, S. F. Ackley, and T. L. DeLiberty (2008), Thickness distribution of Antarctic sea ice, *J. Geophys. Res.*, *113*, C05S92, doi:10.1029/2007JC004254.

Erratum

In the originally published version of this article, the acknowledgments section was incomplete. The missing information has since been corrected and this version may be considered the authoritative version of record.